

Journal of Materials Chemistry C

Accepted Manuscript



This is an *Accepted Manuscript*, which has been through the Royal Society of Chemistry peer review process and has been accepted for publication.

Accepted Manuscripts are published online shortly after acceptance, before technical editing, formatting and proof reading. Using this free service, authors can make their results available to the community, in citable form, before we publish the edited article. We will replace this *Accepted Manuscript* with the edited and formatted *Advance Article* as soon as it is available.

You can find more information about *Accepted Manuscripts* in the [Information for Authors](#).

Please note that technical editing may introduce minor changes to the text and/or graphics, which may alter content. The journal's standard [Terms & Conditions](#) and the [Ethical guidelines](#) still apply. In no event shall the Royal Society of Chemistry be held responsible for any errors or omissions in this *Accepted Manuscript* or any consequences arising from the use of any information it contains.

PAPER

Phase Dependent Visible to Near-Infrared Photoluminescence of CuInS₂ Nanocrystals

Cite this: DOI: 10.1039/x0xx00000x

A. D. P. Leach,^a L. G. Mast,^b E. A. Hernandez-Pagan^b and J. E. Macdonald^{b,*}

Received 00th January 2012,

Accepted 00th January 2012

DOI: 10.1039/x0xx00000x

www.rsc.org/

Nanocrystals of CuInS₂ with the hexagonal wurtzite structure hold great potential for applications requiring efficient energy transport, such as photocatalysis, due to their anisotropic crystal structure. However, thus far their optical properties have proven difficult to study, as luminescence from wurtzite nanocrystals has only recently been observed. In this work, we report the colloidal synthesis of single crystalline, luminescent CuInS₂ nanocrystals with both the cubic and hexagonal structures. The crystalline phase, optical properties and mechanism of formation of nanocrystals are controlled by changing the reaction temperature. Photoluminescence is observed in the visible and near-infrared spectral regions, which results from the cubic and hexagonal nanocrystals respectively. Synthetic studies combined with XRD, TEM and EDS mapping provide evidence for the mechanisms behind phase selection.

Introduction

Semiconductor nanocrystals (NCs) have garnered significant attention from the scientific community due to their tuneable, size-dependent opto-electronic properties and large surface area.^{1, 2} These properties give rise to many potential applications, including use in photovoltaic devices,³ biological sensing,⁴ as catalysts,⁵ and photocatalysts.⁶ Amongst the most commonly studied semiconductor NC systems are the II - VI cadmium chalcogenides.^{7, 8} However, currently these systems are not optimal as the toxicity of Cd leads to concerns about disposal of NC containing devices and limits *in vivo* use.⁹ Further they suffer from photoinstability under the conditions used for water splitting, restricting their use as photocatalysts.^{10, 11} Therefore NC systems with different constituent elements, but similar opto-electronic properties are sought.

Copper indium sulfide (CuInS₂) is a particularly promising alternative to the cadmium chalcogenide systems, due to the lower toxicity of its constituent elements and its high photostability.¹² Further, the material has a direct band gap ~ 1.5 eV in magnitude,¹³ ideally energetically situated for water reduction, and a large optical absorption coefficient ($\alpha > 10^5 \text{ cm}^{-1}$).¹⁴ NCs of CuInS₂ have also shown unexpected phases not observed in the bulk, with nanocrystals reported in three distinct structures: chalcopyrite (CP), zinc blende (ZB), and wurtzite (WZ).^{15, 16} CP, the thermodynamic product seen in the bulk phase, is a tetragonal distortion of the cubic ZB phase. It is also the most commonly produced phase and therefore has been extensively studied.¹⁷⁻²⁰

The hexagonal WZ structure of CuInS₂, only isolable thus far in nanostructures, is particularly interesting as it is anisotropic in the crystallographic *c*-direction.²¹ The exploitation of this anisotropy will improve and control electronic, structural and chemical properties in light-absorbing technologies: the anisotropic electronic structure can be used for orthogonal

charge propagation in solar cell or photocatalyst design;²² the hexagonal crystal structure is being used to grow asymmetric nanocrystals,^{23, 24} which can act as light absorbing antennae;²⁵ the anisotropic surface chemistry can be used to enhance epitaxial interactions to an appropriate substrate and has been used to increase charge transfer rates in solar cell design, improving efficiencies.²⁶

The WZ phase of CuInS₂ nanocrystals was first identified in 2008 by Pan *et al.*²⁷ Since then, WZ CuInS₂ NCs have been synthesized by a variety of methods with a range of accessible morphologies including plates, rods and spheres.²⁷⁻²⁹ Fundamental studies on both cation ordering within the structure³⁰ and the electronic band structure of the material³¹ have been undertaken. However, the luminescence properties of this material have not yet been completely elucidated, as few examples of luminescent WZ NCs have been reported and none synthesized *via* direct methods.³²

The mechanism by which the WZ structure is preferentially formed in colloidal syntheses is not yet fully understood. Several groups have shown evidence of a hexagonal copper sulfide intermediate, possibly achieved through the decomposition of a copper thiolate complex.^{23, 27, 33} Others have evoked the role of stronger metal coordinating agents controlling nucleation kinetics.^{34, 35} Without complete understanding of the mechanism, the production of single crystalline, monodisperse, quantum confined WZ CuInS₂ remains a considerable challenge. Colloidal syntheses often instead yield polytypic NCs or hybrid particles composed of Cu₂S—In₂S₃ or Cu₂S—CuInS₂.^{34, 36-41}

In this paper, single crystalline NCs of CuInS₂ are prepared by a colloidal synthesis through the reaction of In₂S₃ NCs, formed *in situ*, with a Cu—thiolate complex (Figure 1). By changing the reaction temperature, the crystalline phase, optical properties, and mechanism of formation of the product can be controlled. We propose that at low reaction temperature, cubic

CuInS₂ is formed by the intercalation of Cu⁺ ions into the tetragonal In₂S₃ intermediate. At higher reaction temperatures, the In₂S₃ acts only as an In³⁺ reservoir and WZ CuInS₂ NCs are formed by the intercalation of In³⁺ into a hexagonal Cu₂S intermediate. Two distinct regions of emission are observed in the photoluminescence (PL) spectra of these NCs. Emission in the visible region is assigned to ZB CuInS₂.^{17, 28, 42, 43} A broad peak in the near-infrared (NIR) is also observed and correlates to the presence of WZ CuInS₂ nanocrystals in the product.

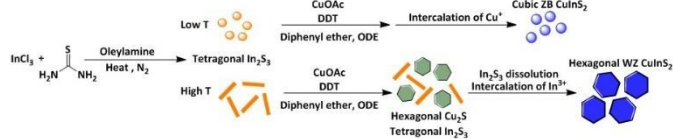


Figure 1. Schematic illustration of the synthesis of CuInS₂ NCs.

This is the first report of WZ CuInS₂, produced using a direct synthesis, with emission in the near-infrared.³² This will facilitate the study of these NCs through luminescence spectroscopies.⁴⁴⁻⁴⁶ The complete understanding of this material's optical properties is key to the realization of its potential in photovoltaic and photocatalytic applications. Furthermore the observation of NIR PL within the tissue transparency window, from NCs with non-toxic constituent elements, shows the promise of WZ CuInS₂ for use in biological applications.

Experimental techniques

Materials

Indium chloride (InCl₃, Alfa Aesar, 99.99%), thiourea (Sigma-Aldrich, ≥ 99.0%), oleylamine (OAm, Aldrich, 70%), copper (I) acetate (CuOAc, Strem Chemicals, 99%), 1-dodecanethiol (DDT, Aldrich, ≥ 98.0%), octadecene (ODE, Aldrich, 90%), diphenyl ether (Sigma-Aldrich, 99%) and *tert*-dodecylmercaptan (*t*-DDT, Aldrich, 98.5%) were purchased and used as received. Standard air-free Schlenk techniques were used throughout with N₂ as the inert gas.

Synthesis of CuInS₂ NCs

CuInS₂ NCs were prepared *via* the reaction scheme shown in Figure 1. Briefly, InCl₃ (111.5 mg, 0.5 mmol) and thiourea (77.5 mg, 1.0 mmol) were added to oleylamine (10 mL) in the reaction vessel, degassed for 1 hr, and heated to the required temperature (115 – 235°C) under a nitrogen atmosphere. Separately CuOAc (65.0 mg, 0.5 mmol) was suspended in ODE (500 μL), diphenyl ether (500 μL) and DDT (240 μL, 1.0 mmol). At the required reaction temperature, 1 mL of the Cu solution was injected quickly (< 1 s) into the reaction vessel. After 30 min, the heat was removed and the reaction mixture was cooled to room temperature. The obtained CuInS₂ NCs were precipitated by addition of methanol/ acetone (v/v, 2:1) and then purified by repeated centrifugation and decantation with addition of methanol/ acetone and hexanes.

Transmission electron microscopy (TEM)

TEM images were collected and energy dispersive x-ray spectroscopy (EDS) was carried out using a FEI Tecnai Osiris™ digital 200 kV S/TEM system. TEM samples were prepared by drop casting a dilute NC solution in hexanes onto a

nickel grid with a carbon support and drying in air at room temperature.

X-ray diffraction (XRD) and Rietveld Refinement

XRD measurements were performed using a Scintag XGEN-4000 X-ray diffractometer with a CuK_α (λ = 0.154 nm) radiation source. The resulting diffraction patterns were then visually compared to literature data to determine the structure.^{36, 47} Rietveld Refinement was performed using the General Structure and Analysis System (GSAS) suite of programs and the EXPGUI interface.⁴⁸⁻⁵⁰ The GSAS suite of programs allows the refinement of parameters including site occupancy, atomic parameters, lattice parameters, background coefficients, peak profiles, atomic displacements and preferred orientation. The quality of the refinement is monitored by visual comparison of calculated and observed patterns, facilitated by plotting a difference curve below the x-axis, and calculating the goodness-of-fit parameter, χ².

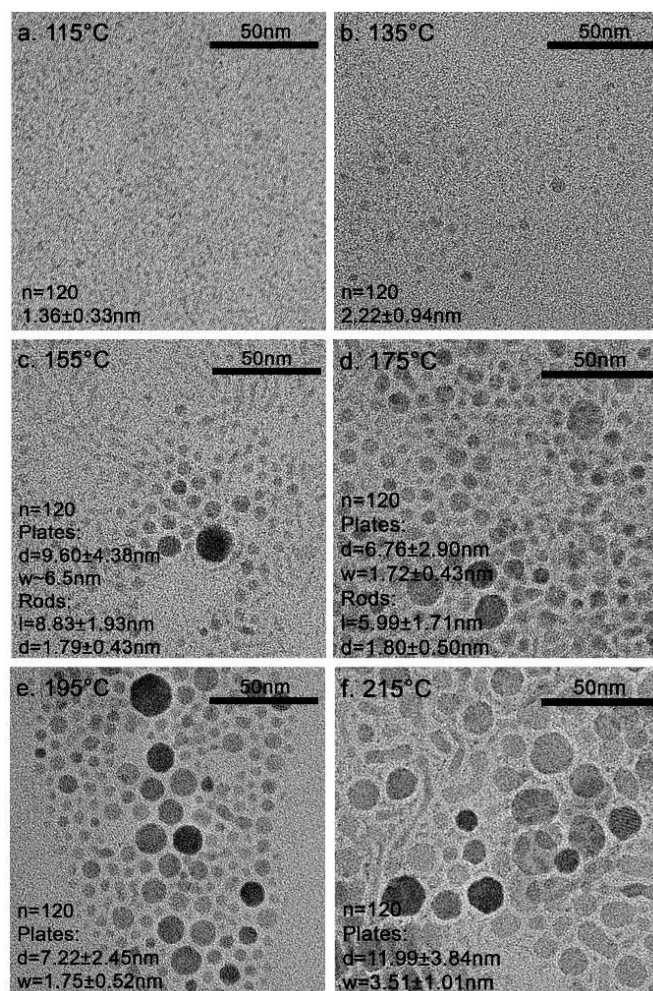


Figure 2. a.-f. TEM images of CuInS₂ NCs prepared at reaction temperatures from 115 - 215°C.

Optical spectroscopy

The absorption spectra of NC samples were collected from 300 – 1400 nm on a UV-visible spectrophotometer (Jasco V-670). Visible PL spectra were measured from 550 – 900 nm on a spectrofluorometer (Jasco FP-8300). NIR PL spectra were

measured from 800 – 1400 nm on a different spectrofluorometer (Jobin Yvon/Horiba Fluorolog-3 FL3-111). Samples were measured in solution with hexanes as the solvent. Both visible and NIR PL were measured with excitation wavelength 348 nm. Data were then matched at 800 nm and normalized to the quantum yield (QY). The QY was determined for each sample by comparison to a Rh-101 standard.⁵¹ Finally data were analysed by using the Fityk application to fit Gaussian functions to emissive peaks.⁵² The goodness of fit parameter, χ^2 , was minimized *via* the Levenberg-Marquardt algorithm.

Results and discussion

Morphology of CuInS₂ NCs

TEM of the product NCs indicated that a variety of morphologies and NC sizes were accessible *via* this synthetic route (Figure 2). At low temperature (115 – 135°C) small, monodisperse, spherical particles (~ 1.5 nm in diameter) were observed that showed an increase in size at the higher temperature. When the reaction temperature was above 135°C, rod- and plate-like products were seen in addition to the small spheres. Both these new morphologies showed increased size with increased reaction temperature, though the rods had a consistent width (1.8 nm). Further, the proportion of plates observed increased with reaction temperature.

Structure & composition of CuInS₂ NCs

In order to determine the structure of the prepared NCs XRD data were collected for each sample (Figure 3a). For samples prepared at 115°C, reflections characteristic of the ZB phase were observed. As the reaction temperature was increased, however, reflections characteristic of the WZ phase increased in intensity, appearing dominant for samples prepared at 215°C and 235°C. This structural trend was confirmed by Rietveld Refinement of the resultant XRD patterns for each reaction temperature (Figure 3b).

An EDS map collected from the sample prepared at 155°C (Figure 3c) indicated that some plate-shaped particles seen at intermediate temperatures consisted of only Cu and S. As a result the Rietveld Refinement used to fit a structural model to the experimental data included three phases: the ZB and WZ CuInS₂ phases reported by Chang *et al.* and the high chalcocite copper sulfide (hiCC Cu₂S) phase reported by Wuensch *et al.*, (Figure S1 and S2).^{36, 47, 50} For samples prepared at 115°C and 135°C, data were fit to within a statistically acceptable tolerance without the addition of the Cu₂S impurity phase (Figure S2).⁵³ Small amounts of WZ and hiCC Cu₂S may be present at these low reaction temperatures, however, crystallite size broadening of the more intense ZB peaks obscures the reflections from these phases.

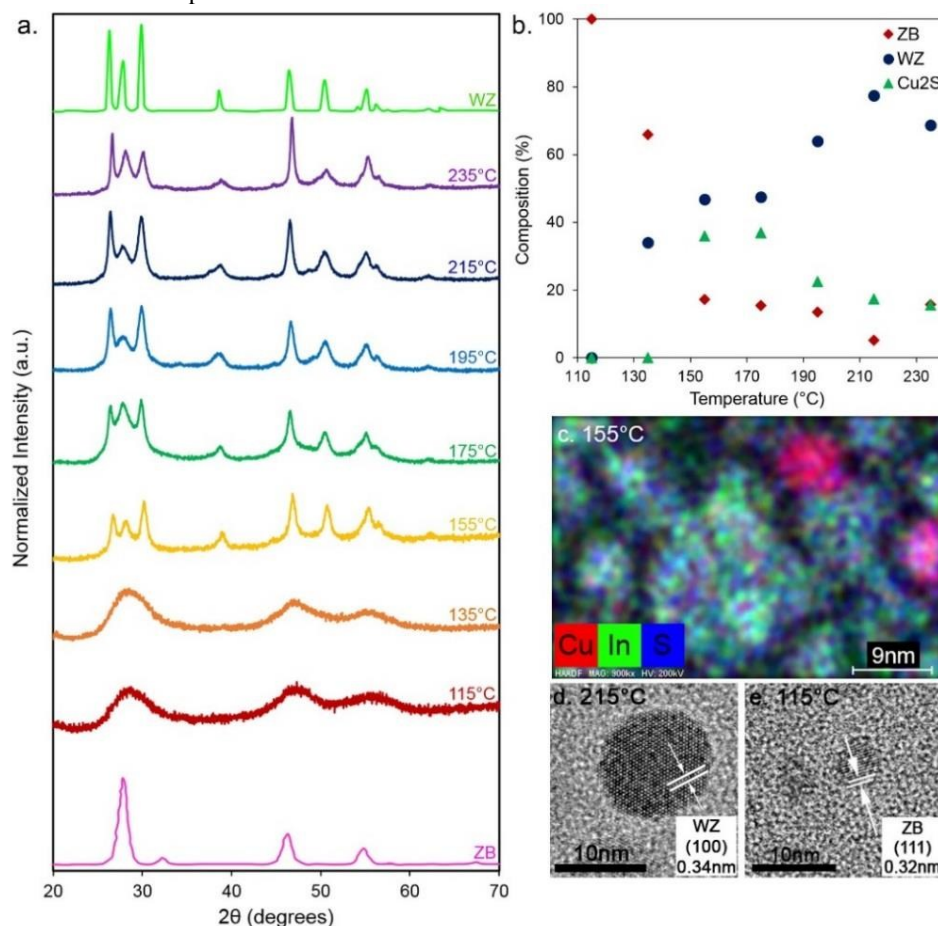


Figure 3. a. XRD of CuInS₂ NCs prepared at various temperatures. Pure ZB and WZ spectra are digitized from the work of Chang *et al.*;³⁶ b. Proportion of WZ (blue), ZB (red) and hiCC Cu₂S (green) phases present in each sample plotted as a function of temperature, as determined by Rietveld Refinement of XRD; c. EDS map of CuInS₂ NCs prepared at 155°C showing the presence of Cu₂S NCs; d.-e. High resolution TEM (HRTEM) images of CuInS₂ NCs prepared at 215°C (plates) and 115°C (spheres) respectively showing lattice fringing.

PAPER

Application of the Scherrer equation to the broadened peaks yielded NC domain sizes in good agreement to those of nanoplates (at high temperatures) and spheres (at low temperatures) measured by TEM for samples prepared below 235°C (Figure S3). This suggests that the NCs are single crystalline, in contrast to many literature examples, which exhibit polytypism.^{40, 41} In order to ensure the prepared NCs were both single phase and single domain HRTEM images of individual NCs were collected. Lattice fringes in HRTEM show that the nanoplates (Figure 3d) are single crystalline with a d-spacing of 0.34 nm indexed to the (100) plane of WZ CuInS₂.²⁸ In contrast, while the smaller spherical NCs (Figure 3e) are also single crystalline, they have a d-spacing of 0.32 nm indexed to the (111) plane of ZB CuInS₂.³⁶

Optical characterization of CuInS₂ NCs

The absorbance spectra for NC samples are shown in Figure 4a. At lower reaction temperatures, the absorbance onset increases with increasing temperature, suggesting that the small NCs obtained at low reaction temperature are quantum confined. Above 175°C, there is no significant change in absorbance onset, indicating that NCs have grown larger than the Wannier-Mott bulk exciton radius of CuInS₂ (~ 4 nm).¹³ This is in good agreement with the average size of NCs, 7 ± 3 nm at 175°C. A Tauc plot (Figure 4b) was used to determine the band gap of the sample prepared at 215°C, which consisted of > 80% WZ phase NCs.^{54, 55} The calculated band gap of 1.56 eV was consistent with the literature value for the WZ phase, 1.55 eV.³⁰

PL spectra were collected for all samples from 550 – 1400 nm and are shown in Figure 4c normalized to the QY. Multiple emissive peaks can be observed in both the visible and NIR spectral regions. At low reaction temperatures, visible emission at ~ 640 nm is dominant, which has been previously reported for ZB CuInS₂, and is consistent with both TEM and XRD analysis.^{17, 42} At high reaction temperature only NIR emission is

observed. It is attributed to WZ CuInS₂, the predominant structure formed at these temperatures.³² The QY was < 0.8% for all samples (Figure S5).

The visible peak, attributed to ZB CuInS₂, was fit to a single Gaussian (Figure S6), which showed a red shift as reaction temperature increased. This is most likely due to an increase in the size of the NCs and the relaxation of quantum confinement conditions. This is consistent with the trends observed in absorbance spectra and reported in literature examples.⁵⁶⁻⁵⁸

The broad, multimodal shape of the NIR PL peak, centred at ~ 950 nm, and the large Stokes shift (0.25 eV) indicate that emission is from several trap states. To identify the energetic location of specific emissive defects, spectra were fit using Fityk, a curve fitting and data analysis application.⁵² The data were fit for all samples by four Gaussians centred at 810, 898, 969 and 1069 nm (Figure S6). A more detailed study of the origin and properties of this PL is currently being undertaken.

Mechanism of formation of prepared CuInS₂ NCs

In order to determine the mechanism of formation of the prepared CuInS₂ NCs, the In—S precursor solution, into which the Cu complex was injected, was examined. At 115°C, TEM images collected (Figure 5c) indicate that small, spherical NCs of In₂S₃ are formed with diameter 1.14 ± 0.36 nm. XRD measurements (Figure 5a) indicate a tetragonal β -In₂S₃ phase (JCPDS card no. 25-0390) with considerable line broadening observed due to the small crystallite size.⁵⁹ EDS analysis showed that the NCs were S deficient with composition In₂S_{2.5}. The ZB CuInS₂ product of the complete reaction (Figure 2) at 115°C is of comparable size (1.36 ± 0.33 nm) to the In₂S₃ precursor and the crystal structures of the two materials are closely related (tetragonal to cubic). It is therefore likely that the ZB CuInS₂ product is formed by the intercalation of Cu⁺ ions into the previously formed β -In₂S₃ NC host (Figure 5c).⁶⁰

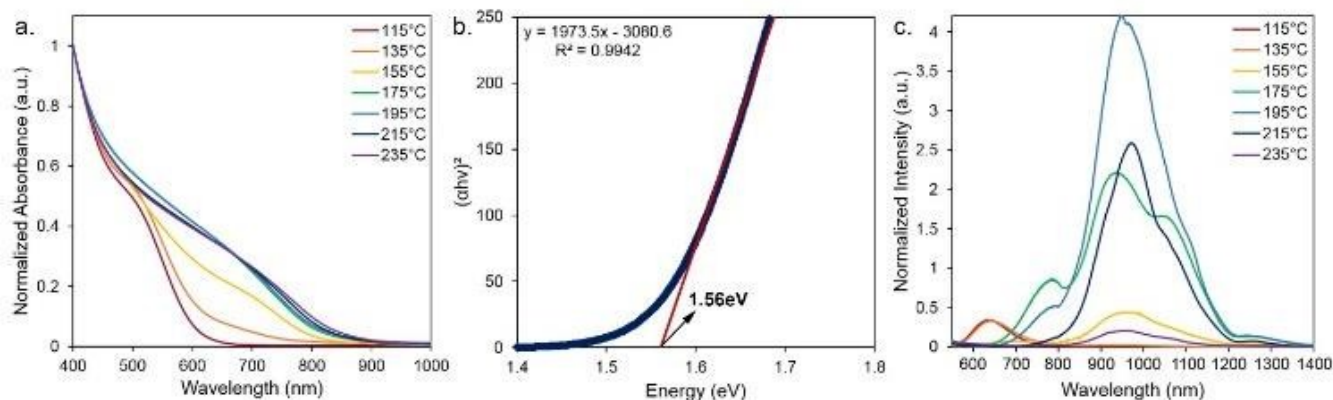


Figure 4. a. Absorbance spectra of CuInS₂ NC dispersions in hexanes prepared at different temperatures; b. Tauc plot of the predominantly WZ CuInS₂ NCs prepared at 215°C; c. PL spectra normalized to the QY of CuInS₂ NC dispersions in hexanes prepared at different temperatures.

PAPER

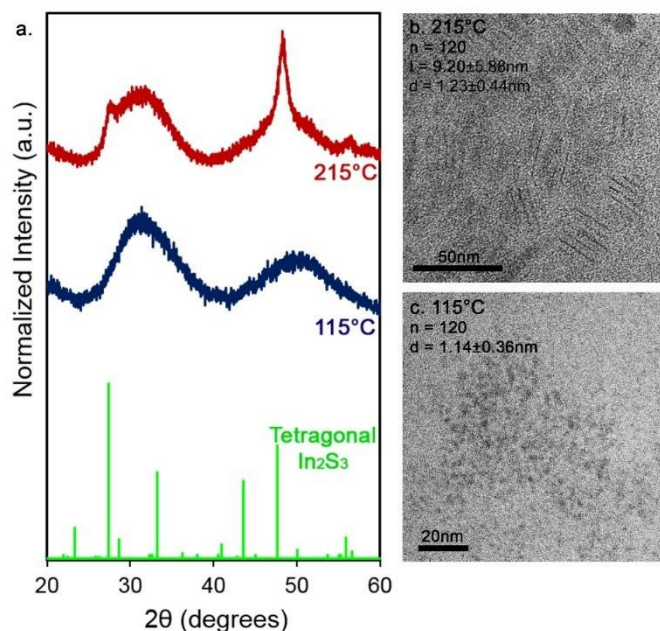


Figure 5. a. XRD patterns collected for In_2S_3 NCs prepared at 115°C and 215°C. Data for tetragonal $\beta\text{-In}_2\text{S}_3$ is from JCPDS card no. 25-0390; b.-c. TEM images for precursor In_2S_3 NCs prepared at 215°C and 115°C respectively.

At a reaction temperature of 215°C, In_2S_3 NCs with rod-like morphology are observed with length 9.20 ± 5.88 nm and diameter 1.23 ± 0.44 nm (Figure 5b). The resulting XRD pattern (Figure 5a) was also indexed to the tetragonal phase, $\beta\text{-In}_2\text{S}_3$. The sharp (1 0 9) and (2 2 12) reflections suggest that rods are elongated in the *c*-direction.^{61, 62} Since the In_2S_3 is in the same phase at both reaction temperature extremes, it is unlikely that intercalation of Cu^+ into tetragonal In_2S_3 is also the mechanism by which the hexagonal WZ CuInS_2 is formed. Moreover, the morphology of the In_2S_3 precursor rods is very different than the CuInS_2 nanoplates. An alternative mechanism is needed to explain the formation of the distinct product crystal structure (WZ) at higher reaction temperature. Literature examples have shown that at reaction temperatures greater than 200°C decomposition of a Cu—thiolate complex can occur yielding a Cu_2S intermediate.⁶³⁻⁶⁷ It was hypothesized that the formation of the WZ CuInS_2 proceeds *via* this mechanism. To confirm the hypothesis, the chemistry of the injected Cu—DDT complex was altered.

At reaction temperature 115°C, the DDT in the Cu solution was replaced by *tert*-dodecyl mercaptan (*t*-DDT). The tertiary carbon adjacent to the thiol in *t*-DDT facilitates the facile decomposition of the Cu—thiolate complex.⁶⁸ Therefore the injection of a Cu—*t*-DDT complex was expected to promote the nucleation of Cu_2S , leading to an increase in the proportion of WZ CuInS_2 formed at lower temperatures. XRD data of the NCs produced (Figure 6a) indicated that indeed the dominant phase was WZ even at the low reaction temperature of 115°C.

TEM images (Figure 6b) showed that the sample was polydisperse with plate-like morphology.

In an additional study, the DDT in the Cu solution was replaced by an equimolar amount of oleylamine (OIAm) at reaction temperature 215°C. If the decomposition of the Cu—DDT complex causes the nucleation of hexagonal Cu_2S , allowing the growth of hexagonal WZ CuInS_2 , the use of a Cu—amine complex should give only the ZB phase. The XRD pattern of the resulting NCs (Figure 6a) was, as expected, indexed to the ZB phase of CuInS_2 . TEM images (Figure 6c) showed that these NCs had a mixture of morphologies with hexagonal and triangular shapes observed. Lattice fringing indicated that these morphologies were not characteristic of a hexagonal phase, but of twinning of the cubic ZB phase. It is therefore clear that the mechanism of WZ formation proceeds *via* the decomposition of the Cu—thiolate complex.

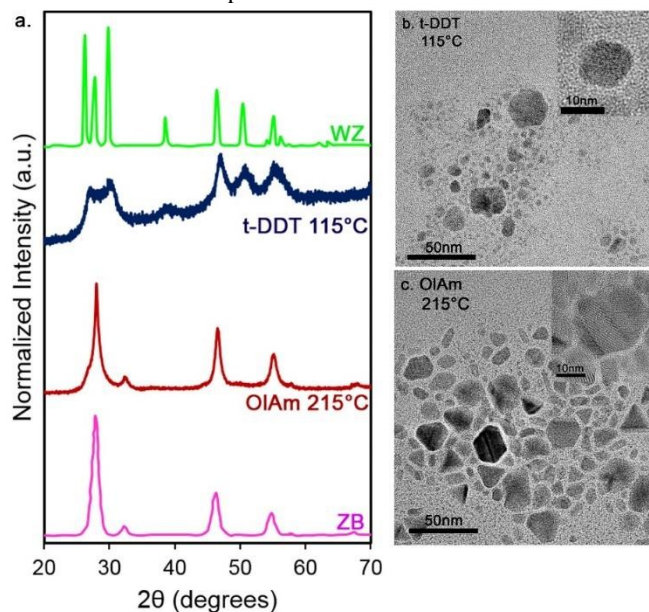


Figure 6. a. XRD patterns collected for CuInS_2 NCs prepared with OIAm as the injection solvent at 215°C and *t*-DDT as the injection solvent at 115°C. Pure ZB and WZ spectra are digitized from the work of Chang *et al.*³⁶ b.-c. TEM images collected for samples prepared with *t*-DDT injection at 115°C and with OIAm injection at 215°C respectively.

To add further support to our mechanistic hypothesis, a detailed aliquot study of the reaction at 215°C was undertaken. Six aliquots of the reaction mixture were taken every 15s from injection of the Cu—DDT complex. The absorbance spectra of the aliquots (Figure 7a) showed a steady increase with temperature in both onset and intensity at larger wavelength. This is indicative of both the size and proportion of WZ CuInS_2 increasing with time. PL measurements were also performed on each aliquot (Figure 7b). Little fluorescence was observed at 15s, suggesting that NCs are not yet completely crystalline, highly defective, or are in the non-fluorescent intermediate

phases Cu_2S and In_2S_3 .^{39, 69} As the reaction progressed a peak in the visible region was observed to grow over the first 30s and then decayed completely by 30 min (Figure 2). We have assigned PL in this region to ZB CuInS_2 and it is thought that this emission is due to some intercalation of Cu into previously formed $\beta\text{-In}_2\text{S}_3$. This observation suggests that the ZB CuInS_2 NCs are a reversible, kinetic product and WZ NCs are more stable at high reaction temperature. Continued heating caused the ZB NCs to dissolve in order for the growth of WZ particles to progress. This hypothesis is supported by the steady increase in intensity of PL in the NIR, which we have assigned to WZ CuInS_2 .

Figure 7c-e show EDS mapping data from aliquots taken at 15s and 75s, and 30 min. Bright field, dark field and elemental analysis images can be found in Figure S8-S9. After 15 s two distinct types of NC were present: nanoplates (diameter 7.40 ± 2.58 nm, depth 3.41 ± 0.53 nm), and nanorods (length 10.03 ± 4.67 nm, diameter 1.51 ± 0.39 nm). EDS mapping showed that the nanoplates were largely composed of Cu and S with some showing small amounts of In present. Lattice fringing in bright field TEM indicated that the nanoplates were single crystalline and had the hiCC Cu_2S structure (Figure S8).³⁸ Literature precedent suggests that the formation of these Cu_2S NCs was due to the decomposition of the Cu—thiolate complex into the Cu_2S intermediate.⁶³⁻⁶⁷ The smaller rods were composed of In and S and were similar in size to the In_2S_3 rods (length 9.26 ± 1.23 nm, diameter 1.23 ± 0.44 nm) observed before injection.

As the reaction progressed, the nanoplates showed a small increase in size (diameter 7.40 ± 2.58 nm, depth 3.41 ± 0.53 nm at 15s; and diameter 8.57 ± 2.68 nm, depth 3.60 ± 1.13 nm at

75s). Further EDS mapping indicated that the proportion of In in the plates also increased with time (Figure 7c-e). This suggests that the hiCC Cu_2S nanoplates are the most stable structure and early stage growth proceeds primarily through the intercalation of In into these NCs. The small In_2S_3 rods decreased in size with time and acted as a reservoir of In^{3+} ions. The large increase in WZ CuInS_2 nanoplate size between 75s (Figure S8) and 30 min (Figure 2) indicates that beyond the initial intercalation step, there is further growth through the addition of more reactant ions and/or Ostwald ripening processes.

In summary, the proposed mechanism of the WZ CuInS_2 formation (Figure 1) is as follows: on injection of the Cu—DDT complex, decomposition of the thiol causes the nucleation of hiCC Cu_2S . Then, as the reaction progresses, the dissolution of the precursor, In_2S_3 rods occurs. Excess In in the reaction mixture intercalates into the hiCC Cu_2S nanoplates forming WZ CuInS_2 . Growth then proceeds until the reaction is quenched. This mechanism is in agreement with a number of literature examples, which report that the formation of WZ CuInS_2 occurs via a Cu_2S intermediate.^{23, 27, 37} While not always explicitly implicated, in all of these examples a thiol is present in the reaction mixture and the reaction temperature is high enough ($\geq 200^\circ\text{C}$) for the decomposition of a Cu—thiolate precursor to occur. Other studies suggest that WZ formation is dependent on the additional presence of a chelating amine ligand that coordinates strongly to the metallic precursors, manipulating the nucleation kinetics.^{34, 35} Reinterpretation with our experiments in mind, suggests that the amine chelates the In^{3+} and allows the formation of the Cu_2S intermediate necessary to WZ- CuInS_2 formation.

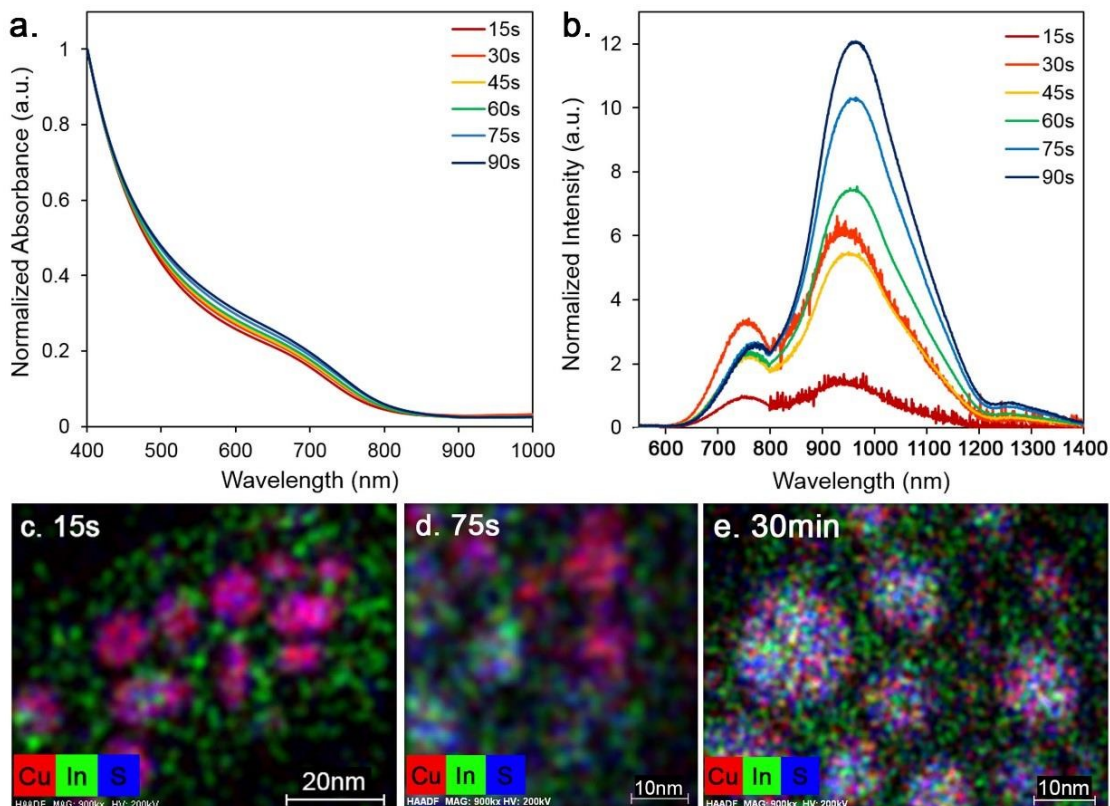


Figure 7. a. Absorbance and b. PL spectra of aliquots taken from the synthesis of CuInS_2 NCs at 215°C ; c.-d. EDS maps of the 15s and 75s aliquots taken from the synthesis of CuInS_2 NCs at 215°C ; e. EDS map of the resultant CuInS_2 NCs produced by the synthesis for 30 min at 215°C .

PAPER

Conclusions

A new synthetic method has been developed that produces WZ CuInS₂ nanoplates with broad emission in the NIR. Samples were multiphase (WZ and ZB) and the presence of both In₂S₃ and hiCC Cu₂S impurities was observed, however, by tuning the reaction temperature the relative proportion of these phases can be controlled. It was further found that the mechanism of WZ CuInS₂ NC formation proceeded *via* intercalation of In³⁺ into a hexagonal Cu₂S intermediate, while ZB CuInS₂ NCs were formed *via* intercalation of Cu⁺ into tetragonal In₂S₃ precursor. Finally we determined that, in order to form the WZ structure, the decomposition of a Cu—thiolate precursor complex was necessary. Our mechanistic insight into the formation of this structure will inform future syntheses, advancing progress towards the production of quantum confined WZ CuInS₂ for solar energy capture.

This paper reports the first example of WZ CuInS₂ NCs, produced using a direct synthesis, with emission in the near-infrared that we are aware of. The observation of PL within the tissue transparency window, from NCs with non-toxic constituent elements, shows the exciting potential of WZ CuInS₂ for use in biological applications. Additionally the observation of PL provides a strong foundation for further study of the optical properties of CuInS₂ *via* luminescence spectroscopies. An understanding of these properties is indispensable in advancing work towards the use of this material in both photocatalytic and photovoltaic applications.

Acknowledgements

This project was supported by the IMS program at Vanderbilt University, NSF Career Award Sus-ChEM-1233105, and the U.S.-Israel Binational Science Foundation. Portions of this work were performed at the Vanderbilt Institute of Nanoscale Science and Engineering, using facilities renovated under TN-SCORE (DMR 0907619) and NSF EPS-1004083.

Notes and references

^a Department of Interdisciplinary Materials Science, Vanderbilt University, Nashville, Tennessee 37235, United States.

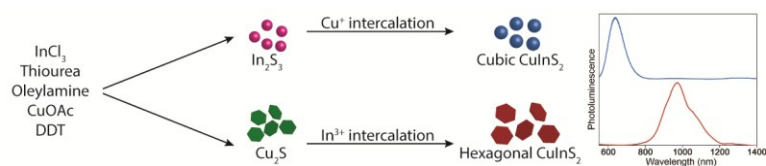
^b Department of Chemistry, Vanderbilt University, Nashville, Tennessee 37235, United States.

Electronic Supplementary Information (ESI) available: complete Rietveld Refinement parameters; Scherrer line broadening crystallite size compared to TEM size; EDS data; quantum yields; Fityk peak fitting parameters; absorbance spectra of hexanes; TEM images from aliquot study; complete EDS maps for aliquot study, including dark field and elemental analysis data. See DOI: 10.1039/b000000x/

- M. A. El-Sayed, *Accounts of Chemical Research*, 2004, **37**, 326.
- A. Eychmuller, *Journal of Physical Chemistry B*, 2000, **104**, 6514.
- M. R. Kim, Z. Xu, G. Chen and D. Ma, *Chemistry-A European Journal*, 2014, **20**, 11256.

- W. J. Parak, D. Gerion, T. Pellegrino, D. Zanchet, C. Micheel, S. C. Williams, R. Boudreau, M. A. Le Gros, C. A. Larabell and A. P. Alivisatos, *Nanotechnology*, 2003, **14**, R15.
- L. L. Chng, N. Erathodiyil and J. Y. Ying, *Accounts of Chemical Research*, 2013, **46**, 1825.
- A. Vaneski, J. Schneider, A. S. Susa and A. L. Rogach, *Journal of Photochemistry and Photobiology C-Photochemistry Reviews*, 2014, **19**, 52.
- A. C. C. Esteves and T. Trindade, *Current Opinion in Solid State & Materials Science*, 2002, **6**, 347.
- N. V. Hullavarad, S. S. Hullavarad and P. C. Karulkar, *Journal of Nanoscience and Nanotechnology*, 2008, **8**, 3272.
- B. A. Rzigalinski and J. S. Strobl, *Toxicology and Applied Pharmacology*, 2009, **238**, 280.
- F. E. Osterloh, *Chemistry of Materials*, 2008, **20**, 35.
- A. Vaneski, A. S. Susa, J. Rodriguez-Fernandez, M. Berr, F. Jaeckel, J. Feldmann and A. L. Rogach, *Advanced Functional Materials*, 2011, **21**, 1547.
- L. Li, T. J. Daou, I. Texier, C. Tran Thi Kim, L. Nguyen Quang and P. Reiss, *Chemistry of Materials*, 2009, **21**, 2422.
- J. Kolny-Olesiak and H. Weller, *ACS Applied Materials & Interfaces*, 2013, **5**, 12221.
- W. J. Yue, S. K. Han, R. X. Peng, W. Shen, H. W. Geng, F. Wu, S. W. Tao and M. T. Wang, *Journal of Materials Chemistry*, 2010, **20**, 7570.
- X. T. Lu, Z. B. Zhuang, Q. Peng and Y. D. Li, *CrystEngComm*, 2011, **13**, 4039.
- M. Booth, A. P. Brown, S. D. Evans and K. Critchley, *Chemistry of Materials*, 2012, **24**, 2064.
- H. Nakamura, W. Kato, M. Uehara, K. Nose, T. Omata, S. Otsuka-Yao-Matsuo, M. Miyazaki and H. Maeda, *Chemistry of Materials*, 2006, **18**, 3330.
- R. Klenk, J. Klaer, R. Scheer, M. C. Lux-Steiner, I. Luck, N. Meyer and U. Ruhle, *Thin Solid Films*, 2005, **480**, 509.
- H. Zhong, S. S. Lo, T. Mirkovic, Y. Li, Y. Ding, Y. Li and G. D. Scholes, *ACS Nano*, 2010, **4**, 5253.
- J. S. Niezgodá, M. A. Harrison, J. R. McBride and S. J. Rosenthal, *Chemistry of Materials*, 2012, **24**, 3294.
- X. Sheng, L. Wang, Y. P. Luo and D. R. Yang, *Nanoscale Research Letters*, 2011, **6**.
- P. R. Sajanlal, T. S. Sreeprasad, A. K. Samal and T. Pradeep, *Nano Reviews*, 2011.
- J. Li, M. Bloemen, J. Parisi and J. Kolny-Olesiak, *ACS Applied Materials & Interfaces*, 2014.
- C. Coughlan, A. Singh and K. M. Ryan, *Chemistry of Materials*, 2013, **25**, 653.
- Y. Shemesh, J. E. Macdonald, G. Menagen and U. Banin, *Angewandte Chemie-International Edition*, 2011, **50**, 1185.
- W. Yue, G. Zhang, S. Wang, W. Sun, M. Lan and G. Nie, *Materials Science in Semiconductor Processing*, 2014, **25**, 337.
- D. Pan, L. An, Z. Sun, W. Hou, Y. Yang, Z. Yang and Y. Lu, *Journal of the American Chemical Society*, 2008, **130**, 5620.
- S. K. Batabyal, L. Tian, N. Venkatram, W. Ji and J. J. Vittal, *Journal of Physical Chemistry C*, 2009, **113**, 15037.
- M. Kruszynska, H. Borchert, J. Parisi and J. Kolny-Olesiak, *Journal of Nanoparticle Research*, 2011, **13**, 5815.
- X. Shen, E. A. Hernández-Pagan, W. Zhou, Y. S. Puzyrev, J.-C. Idrobo, J. E. Macdonald, S. J. Pennycook and S. T. Pantelides, *Nature Communications*, 2014, **5**.
- S. Tomic, L. Bernasconi, B. G. Searle and N. M. Harrison, *Journal of Physical Chemistry C*, 2014, **118**, 14478.
- C. de Mello Donegá, *Chemistry of Materials*, 2014.
- S. T. Connor, C.-M. Hsu, B. D. Weil, S. Aloni and Y. Cui, *Journal of the American Chemical Society*, 2009, **131**, 4962.

- 34 W.-C. Huang, C.-H. Tseng, S.-H. Chang, H.-Y. Tuan, C.-C. Chiang, L.-M. Lyu and M. H. Huang, *Langmuir*, 2012, **28**, 8496.
- 35 K. Nose, Y. Soma, T. Omata and S. Otsuka-Yao-Matsuo, *Chemistry of Materials*, 2009, **21**, 2607.
- 36 J. Chang and E. R. Waclawik, *CrystEngComm*, 2013, **15**, 5612.
- 37 S. T. Connor, C.-M. Hsu, B. D. Weil, S. Aloni and Y. Cui, *Journal of the American Chemical Society*, 2009, **131**, 4962.
- 38 J.-Y. Chang and C.-Y. Cheng, *Chemical Communications*, 2011, **47**, 9089.
- 39 W. Han, L. Yi, N. Zhao, A. Tang, M. Gao and Z. Tang, *Journal of the American Chemical Society*, 2008, **130**, 13152.
- 40 B. Koo, R. N. Patel and B. A. Korgel, *Chemistry of Materials*, 2009, **21**, 1962.
- 41 Z. P. Liu, L. L. Wang, Q. Y. Hao, D. K. Wang, K. B. Tang, M. Zuo and Q. Yang, *CrystEngComm*, 2013, **15**, 7192.
- 42 V. K. Komarala, C. Xie, Y. Wang, J. Xu and M. Xiao, *Journal of Applied Physics*, 2012, **111**.
- 43 Y. Chen, S. Li, L. Huang and D. Pan, *Inorganic Chemistry*, 2013, **52**, 7819.
- 44 M. Jones and G. D. Scholes, *Journal of Materials Chemistry*, 2010, **20**, 3533.
- 45 W. Zhang and X. Zhong, *Inorganic Chemistry*, 2011, **50**, 4065.
- 46 L. Li, A. Pandey, D. J. Werder, B. P. Khanal, J. M. Pietryga and V. I. Klimov, *Journal of the American Chemical Society*, 2011, **133**, 1176.
- 47 B. J. Wuensch and M. J. Buerger, *Mineralogical Society of America*, 1963, **1**, 164.
- 48 H. M. Rietveld, *Journal of Applied Crystallography*, 1969, **2**, 65.
- 49 A. C. Larson and R. B. Von Dreele, Los Alamos National Laboratory Report LAUR 86-748, 1994.
- 50 B. H. Toby, *Journal of Applied Crystallography*, 2001, **34**, 210.
- 51 K. Rurack and M. Spieles, *Analytical Chemistry*, 2011, **83**, 1232.
- 52 M. Wojdyr, *Journal of Applied Crystallography*, 2010, **43**, 1126.
- 53 B. H. Toby, *Powder Diffraction*, 2006, **21**, 67.
- 54 X. Lu, Z. Zhuang, Q. Peng and Y. Li, *Chemical Communications*, 2011, **47**, 3141.
- 55 J. Tauc, Grigorov.R and A. Vancu, *Physica Status Solidi*, 1966, **15**, 627.
- 56 D. Deng, Y. Chen, J. Cao, J. Tian, Z. Qian, S. Achilefu and Y. Gu, *Chemistry of Materials*, 2012, **24**, 3029.
- 57 R. Xie, M. Rutherford and X. Peng, *Journal of the American Chemical Society*, 2009, **131**, 5691.
- 58 T. Pons, E. Pic, N. Lequeux, E. Cassette, L. Bezdetnaya, F. Guillemin, F. Marchal and B. Dubertret, *ACS Nano*, 2010, **4**, 2531.
- 59 A. Weibel, R. Bouchet, F. Boule'h and P. Knauth, *Chemistry of Materials*, 2005, **17**, 2378.
- 60 M. Ge, C. Guo, L. Liu, B. Zhang and Z. Zhou, *Australian Journal of Chemistry*, 2009, **62**, 1690.
- 61 Y. H. Kim, J. H. Lee, D.-W. Shin, S. M. Park, J. S. Moon, J. G. Nam and B. Yoo, *Chemical Communications*, 2010, **46**, 2292.
- 62 Y. Xing, H. Zhang, S. Song, J. Feng, Y. Lei, L. Zhao and M. Li, *Chemical Communications*, 2008, 1476.
- 63 T. Kino, T. Kuzuya, K. Itoh, K. Sumiyama, T. Wakamatsu and M. Ichidate, *Materials Transactions*, 2008, **49**, 435.
- 64 M. J. Turo and J. E. Macdonald, *ACS Nano*, 2014, **8**, 10205.
- 65 W. Bryks, M. Wette, N. Velez, S.-W. Hsu and A. R. Tao, *Journal of the American Chemical Society*, 2014, **136**, 6175.
- 66 P. L. Saldanha, R. Brescia, M. Prato, H. Li, M. Povia, L. Manna and V. Lesnyak, *Chemistry of Materials*, 2014, **26**, 1442.
- 67 T. H. Larsen, M. Sigman, A. Ghezelbash, R. C. Doty and B. A. Korgel, *Journal of the American Chemical Society*, 2003, **125**, 5638.
- 68 M. Kruszynska, H. Borchert, A. Bachmatiuk, M. H. Rummeli, B. Büchner, J. Parisi and J. Kolny-Olesiak, *ACS Nano*, 2012, **6**, 5889.
- 69 J. J. Ning, K. K. Men, G. J. Xiao, L. Y. Zhao, L. Wang, B. B. Liu and B. Zou, *Journal of Colloid and Interface Science*, 2010, **347**, 172.

ToC graphic:**ToC text:**

Here the first synthesis that produces CuInS₂ nanocrystals with tuneable photoluminescence from the visible to near-infrared spectral regions is demonstrated.